



# Pyrolysis characteristics and kinetic analysis of tobacco stem pretreated with different solvents

Xiao Li<sup>1</sup> · Qingqing Zhao<sup>1</sup> · Ming Han<sup>2</sup> · Ke Zhang<sup>3</sup> · Zhongya Guo<sup>3</sup> · Bin Li<sup>3</sup> · Wei Wang<sup>1</sup> · Xuhe Wei<sup>1</sup> · Miao Liang<sup>1</sup>

Received: 8 October 2021 / Revised: 20 December 2021 / Accepted: 23 December 2021 / Published online: 4 January 2022  
© The Author(s), under exclusive licence to Springer-Verlag GmbH Germany, part of Springer Nature 2022

## Abstract

In the present study, the effects of pretreatments with different solvents (hydrochloric acid, sodium hydroxide, and ethanol) on the physicochemical structure and pyrolysis behavior of tobacco stem (TS) were investigated. Elemental compositions analysis showed that acid washing increased the carbon content and exhibited a high removal percentage for the inorganic species. SEM, BET, and FTIR analysis showed that the pretreatments exerted different effect on the surface and microstructure. Furthermore, the pyrolysis characteristics analysis indicated that solvent pretreatment increased the initial pyrolysis temperature due to the removal of unstable volatile components, especially for the acid and alkali washing samples. Meanwhile, hydrochloric acid pretreatment increased the maximum pyrolysis rate temperature of cellulose decomposition stage and decreased the char residues due to the large removal of inorganic species, while alkali treatment produced the opposite result. Pyrolysis kinetic analysis based on Coats-Redfern method showed that F1.5 chemical reaction model can be used to describe the pyrolysis stages of TS samples and a decreased activation energy was observed during the decomposition of cellulose stage for the acid and alkali washed samples. The released gaseous products during the pyrolysis process were also monitored by using TG-FTIR technique, and the gaseous release behavior was different from each other.

**Keywords** Tobacco stem · Solvent pretreatment · Pyrolysis characteristics · Kinetic analysis · TG-FTIR

## 1 Introduction

Tobacco is a worldwide special economic crop. In China, the area of tobacco cultivation was about 1.3 million hectares with a tobacco leaf production of 2.8 million tonnes according to the website <http://www.statista.com>. During the cigarette manufacturing process, tobacco stem (TS) is the discarded waste due to its non-applicability and accounting for about 25% of the tobacco leaves [1]. Most of the TS is disposed by landfill or direct incineration, leading to the waste of resources and environmental pollution problems.

In fact, similar to other lignocellulosic biomass, the TS is mainly composed of cellulose, hemicellulose, lignin, and other organic matter. Many high value-added products can be produced through the pyrolysis of biomass, such as bio-oil, syngas, and biochar [2]. Bio-oil and syngas possess high heating values and can be used as high-quality transportation fuels after refining [3–7]. Biochar can be used for the production of fuel [8], activated carbon [9], and new fertilizer [10–12]. Therefore, the rational utilization of tobacco waste resources for the production of value-added products is highly desirable, which could both broaden the selection range of biomass feedstock and alleviate energy and environmental problems [13, 14].

Several studies have focused on the pyrolysis of tobacco waste. Chen et al. [15] investigated the co-pyrolysis of tobacco stalk with different types of polymer wastes. The synergistic effect compared to the pyrolysis of the individual components was observed, which could increase carbon conversion efficiency and volatiles yield. Strezov et al. [16] reported that the pyrolysis process of tobacco waste can be divided into four stages according to the derivative thermogravimetric curve, that is

✉ Zhongya Guo  
zhongyaguo@126.com

✉ Miao Liang  
liangmiaozu@163.com

<sup>1</sup> School of Food and Biological Engineering, Zhengzhou University of Light Industry, Zhengzhou 450001, China

<sup>2</sup> Anyang Cigarette Factory, China Tobacco Henan Industrial Co., Ltd, Anyang 455000, China

<sup>3</sup> Zhengzhou Tobacco Research Institute of CNTC, Zhengzhou 450001, China

dehydration, torrefaction, charring, and carbonization. In fact, the structural characteristic and chemical composition of raw biomass have an important influence on the pyrolysis process and resulting products. Compared with other biomass, TS exhibits unique properties due to its high content of alkaloid (mainly nicotine), alkali, and alkaline earth metals (especially the potassium). A previous work suggested that the alkaloid can be released and transferred to bio-oil under 400 °C, resulting in potential environmental contamination and waste of valuable chemicals [17]. Meanwhile, the potassium is inconvenient for the pyrolysis process due to its slagging and fouling shortcomings [18]. Therefore, leaching of alkaloids and inorganic species from the TS prior to pyrolysis process is necessary.

Many studies have indicated that leaching pretreatment can improve the quality of biomass pyrolysis products [19, 20]. For example, acid washing can effectively remove alkali and alkaline earth metals from the biomass, resulting in the reduction of catalytic reactions and pyrolytic slagging [21, 22]. Meanwhile, acid washing degraded partial hemicellulose in biomass, which can reduce the production of acetic acid and diminish the acidity of bio-oil [23]. Chen et al. [24] found that nicotine and inorganic species in TS were almost completely removed by acid leaching and the thermal stability of TS was decreased due to the damaged matrix structure. In addition, alkali washing is also an effective pretreatment method to change the fiber structure and compositions through the solubilization of cellulose and lignin [25]. For instance, Dalle et al. [26] employed the sodium hydroxide pretreatment method to partially remove amorphous compounds such as lignin, hemicellulose, and extracts and increased the thermal stability.

From the above mentioned studies, it can be concluded that most of the previous studies focused on the effect of a single pretreatment method on the pyrolysis characteristics of different raw materials. Few studies have compared the effect of different solvents pretreatment on the physicochemical characteristics and pyrolysis properties of TS. Therefore, in this study, the influence of pretreatment with different solvents (hydrochloric acid, sodium hydroxide, ethanol) on the physicochemical structure, pyrolysis characteristics, as well as the release behavior of pyrolysis gaseous of TS, was investigated. Coats-Redfern method based on the thermogravimetric data was also applied to determine and compare the pyrolysis kinetic parameters of TS. Furthermore, the release behavior of volatile products during the pyrolysis of TS was monitored by thermogravimetry-Fourier transform infrared analysis (TG-FTIR) technique. The study would pave the way for the rational utilization of waste TS through thermochemical conversion combined with pretreatments.

## 2 Materials and methods

### 2.1 Materials

TS used in this work was obtained from Anyang Cigarette Factory, Henan Province, China. High-purity hydrochloric acid (37.0%), sodium hydroxide ( $\geq 96.0\%$ ), and ethanol ( $\geq 99.7\%$ ) were purchased from Aladdin Chemical Reagent Inc. of Shanghai, China.

### 2.2 Washing pretreatment of TS

Samples of the TS feedstock were firstly cleaned with distilled water to remove surface dust, in order to eliminate the influence of impurities on the experiment results. And then approximately 50 g of TS feedstock ( $m_0$ ) was immersed in 500 mL of water, hydrochloric acid (3.0%), sodium hydroxide (3.0%), and ethanol (75.0%) for 6 h, respectively. Note that the leaching solutions were performed at room temperature. After that, the treated TS samples were washed with distilled water 3 times. Next, all four samples were placed into a drying oven at 60 °C for 12 h to remove the excessive water and avoid changing volatile components. The mass of each sample after drying ( $m_i$ ) was weighted for the calculation of mass retention rate (MRR,  $MRR = m_i/m_0$ ). Finally, the dried samples were crushed by a multifunctional disintegrator (DSY500A, Zhuokai electric appliance, China) and sieved by 60 mesh (0.3 mm) sieve, the resulting samples were denoted as the raw TS, TS-H, TS-OH, and TS-EtOH, respectively.

### 2.3 Composition and structure analysis

The organic elemental analysis (dry basis by wt%) was carried out using an elemental analyzer (Vario EL-III CHNS, Germany). The content of oxygen was calculated by difference. The inorganic elemental contents, such as K, Ca, Na, and Mg of the TS and pretreated TS samples, were determined by using inductively coupled plasma optical emission spectroscopy (ICP-OES, Agilent 730, USA). The surface morphology of the samples was observed by using scanning electron microscopy (SEM, SU8100) worked at 3.0 kV voltage. The Brunauer-Emmett-Teller (BET, ASAP 2020, Micromeritics) was used to determine the surface area under  $N_2$  isothermal (77 K) adsorption. The samples were degasified at 120 °C for 6 h under vacuum before  $N_2$  adsorption. Fourier transform infrared spectroscopy (FTIR) analysis of the samples was performed using an FTIR spectrometer (Nicolet 6700, Thermo Scientific) in the range of 400–4000  $cm^{-1}$  with a pure KBr pellet as background.

## 2.4 Thermogravimetric experiments

Thermogravimetric analysis of the raw TS and pretreated TS samples was carried out using a thermogravimetric analyzer (TGA, Q5000, USA). For the pyrolysis experiment, approximately 10 mg sample was loaded into a platinum crucible and heated from 40 to 850 °C under the heating rates of 10, 20, and 40 °C/min in dynamic nitrogen with a flow rate of 25 mL/min. The characteristic pyrolysis parameters, such as initial pyrolysis temperature ( $T_i$ ), the maximum pyrolysis rate temperature ( $T_{max}$ ), the maximum pyrolysis rate ( $DTG_{max}$ ), and final pyrolysis temperature ( $T_f$ ), were determined from the TG and derivative thermogravimetry (DTG, first-order derivative of TG curve) profiles according to a previous study [27]. Then the residual char content ( $\eta$ ) was the proportion of residual mass at the end of the pyrolysis process for the different samples. In addition, the comprehensive pyrolysis index (CPI) can be calculated from the following formula [28]:

$$CPI = \frac{DTG_{max}}{T_{max} \times (T_f - T_i)} \quad (1)$$

Furthermore, the release of gaseous products during the pyrolysis process of raw and washed TS samples was monitored through a thermogravimetric analyzer (Netzsch TG 209F3) coupled with FTIR spectrometry (Nicolet 8700; Thermo Electron, America). The loading amount of samples and atmosphere of furnace chamber were consistent with the above TG experiments at a heating rate of 20 °C/min. The temperature of the transfer line between the TG and FTIR apparatuses was set at 210 °C to prevent the condensation. The resolution of the FTIR was set at 4 cm<sup>-1</sup>, spectrum scan frequency was 8 times per minute, and the spectral region was in the range of 400–4000 cm<sup>-1</sup>.

## 2.5 Pyrolysis kinetic analysis

The pyrolysis of TS samples can be considered a typical inhomogeneous reaction, and the decomposition rate can be described by the following equation:

$$\frac{d\alpha}{dt} = k(T)f(\alpha) \quad (2)$$

$$\alpha = \frac{(m_i - m)}{(m_i - m_f)} \quad (3)$$

where  $\alpha$  is the thermal conversion fraction at moment  $t$  during the pyrolysis process;  $m_i$ ,  $m$ , and  $m_f$  are the initial, instantaneous, and final masses of the samples, which can be obtained from the TG data, respectively;  $f(\alpha)$  represents

the general expression of the reaction model; and the reaction rate constant  $k(T)$  can be obtained from the following Arrhenius equation:

$$k(T) = A \exp\left(-\frac{E_a}{RT}\right) \quad (4)$$

where  $A$  is the frequency factor,  $E_a$  is the activation energy,  $R$  is the universal gas constant (8.314 J·mol<sup>-1</sup>·K<sup>-1</sup>), and  $T$  is the thermodynamic temperature.

The heating rate  $\beta$  is defined as  $dT/dt$ , and then Eqs. (2) and (4) can be combined and rearranged as

$$\frac{d\alpha}{dT} = \frac{A}{\beta} \exp\left(-\frac{E_a}{RT}\right) f(\alpha) \quad (5)$$

The integral form of Equation (5) can be expressed as follows:

$$G(\alpha) = \int_0^\alpha \frac{d\alpha}{f(\alpha)} = \int_{T_0}^T \frac{A}{\beta} \exp\left(-\frac{E_a}{RT}\right) dT \quad (6)$$

where  $G(\alpha)$  is the integral equation of the reaction model  $f(\alpha)$ .

According to Eqs. (2)–(6), different integral kinetic models can be used to calculate the pyrolysis process of TS samples. In this work, the Coats-Redfern method is used to calculate the reaction kinetic equation and parameters for the different TS biomass. By adopting this method, Equation (6) can be transformed into the following logarithmic form:

$$\ln \left[ \frac{G(\alpha)}{T^2} \right] = \ln \left[ \frac{AR}{\beta E_a} \left( 1 - \frac{2RT}{E_a} \right) \right] - \frac{E_a}{RT} \quad (7)$$

There is a linear relationship between  $\ln \left[ \frac{G(\alpha)}{T^2} \right]$  and  $1/T$  due to  $\left( 1 - \frac{2RT}{E_a} \right) \approx 1$ . The model with the highest degree of linearity was selected as the most suitable model. Table 1 lists the common reaction equations and functions for  $G(\alpha)$  in the Coats-Redfern model.

## 3 Results and discussion

### 3.1 Composition and structure analysis of the samples

Generally, solvents pretreatment could affect the composition and structure of biomass, leading to a mass reduction of samples. The MRRs of TS, TS-H, TS-OH, and TS-EtOH were 89.96%, 62.68%, 74.60%, and 89.43% respectively, indicating a different dissolution effect of various solvents. The soluble components were dissolved during the solvents treatment, which may lead to the destruction of the raw TS

**Table 1** Several common solid-phase reaction kinetic model expressions [29, 30]

Reaction model	Reaction mechanism	$f(\alpha)$	$G(\alpha)$	Symbol
Chemical reaction	First-order reaction	$1-\alpha$	$-\ln(1-\alpha)$	F1
	1.5-order reaction	$(1-\alpha)^{3/2}$	$2[(1-\alpha)^{-1/2}-1]$	F3/2
	Second-order reaction	$(1-\alpha)^2$	$(1-\alpha)^{-1}-1$	F2
Diffusion-controlled reaction	One-dimensional diffusion	$1/2\alpha$	$\alpha^2$	D1
	Two-dimensional diffusion	$[-\ln(1-\alpha)]^{-1}$	$(1-\alpha)\ln(1-\alpha)+\alpha$	D2
	Three-dimensional diffusion	$3/2(1-\alpha)^{2/3}[1-(1-\alpha)^{1/3}]^{-1}$	$[1-(1-\alpha)^{1/3}]^2$	D3
Phase boundary reaction	One-dimensional	1	$\alpha$	R1
	Two-dimensional	$2(1-\alpha)^{1/2}$	$1-(1-\alpha)^{1/2}$	R2
	Three-dimensional	$3(1-\alpha)^{2/3}$	$1-(1-\alpha)^{1/3}$	R3

**Table 2** Organic elemental analysis of the TS samples

Sample	Organic elemental analysis (wt/%)					Atomic ratio	
	C	N	H	S	O	O/C	H/C
TS	36.44	1.53	5.53	0.13	56.37	1.55	0.15
TS-H	40.70	1.37	4.17	0.04	53.72	1.32	0.10
TS-OH	38.75	1.02	4.29	0.02	55.92	1.51	0.11
TS-EtOH	37.53	1.31	5.06	0.07	56.03	1.49	0.13

structure. Table 2 shows the result of the ultimate analysis of the raw and washed TS samples. The contents of carbon, nitrogen, hydrogen, sulfur, and oxygen in raw TS were 36.44%, 1.53%, 5.53%, 0.13%, and 56.37%, respectively. Pretreatment with different solvents exhibited different effect on the contents of organic elements. The carbon contents increased at different degrees with the expense of hydrogen and oxygen contents after solvent pretreatment; it may be owing to the dissolution and extraction effect of organic components such as polysaccharides/polyphenols/pectin in the TS. Especially for the TS-H sample, the content of carbon increased significantly to 40.70%, while the hydrogen and oxygen contents decreased to 4.17% and 53.72%, respectively. Correspondingly, both the O/C and H/C atomic ratios of solvent washed TS samples showed a decreasing trend, which could influence the effective heating values of samples. In addition, the contents of nitrogen and sulfur were also decreased after the pretreatment. It is generally believed that biomass with low O/C, H/C, nitrogen, and sulfur could be regarded as clean fuels because of the lower energy loss and emission of  $\text{NO}_x$  and  $\text{SO}_x$  during the combustion process [31].

The contents of inorganic elements were also determined to compare the effect of different solvents washing on the TS. The result of inorganic elemental analysis is shown in Table 3. It can be seen that the raw TS exhibited a high contents of K and Ca of  $4.43 \times 10^{-4}\%$  and  $1.57 \times 10^{-4}\%$ , respectively. It revealed that minerals in TS were mainly consisted of potassium and calcium salts. After acid washing, all the inorganic species in raw TS were removed at different degrees. And among the different solvents washing

**Table 3** Inorganic elemental analysis of the TS samples (wt%  $\times 10^{-4}$ )

Sample	K	Ca	Mg	P	Na
TS	4.43	1.57	0.31	0.20	0.08
TS-H	1.63	0.89	0.17	0.12	0.02
TS-OH	2.34	1.49	0.30	0.19	0.26
TS-EtOH	3.75	1.53	0.31	0.16	0.05

method, the acid washing exhibited a high removal percentage for all the detected inorganic element. For instance, the removal percentage of K was 63.21%, indicating that acid pretreatment had the strongest demineralization effect [32]. Moreover, the removal percentages of K in TS-OH and TS-EtOH were 47.18% and 15.35%, respectively, whereas the content of Ca and Mg did not change significantly, suggesting that Ca and Mg were resistant to alkali and alcohol washing. It was also found that sodium hydroxide washing led to impregnation with Na and resulted in a high Na content in TS-OH sample. Previous study reported that the removal of inorganic species from biomass could improve fuel quality and influence the distribution of pyrolysis products [33]. Therefore, pretreatment with different solvents here may exert different effect on the pyrolysis behavior of TS.

SEM analysis was also conducted to observe the morphology changes of the TS samples. As can be seen from Fig. 1, the raw TS and TS-EtOH exhibited a relatively integrated fibrous structure with a smooth surface, which was the typical structure feature of lignocellulosic biomass, while as for the TS-H and TS-OH samples, the intact



**Fig. 1** SEM images of the raw and washed TS samples: **a** TS; **b** TS-H; **c** TS-OH; **d** TS-EtOH

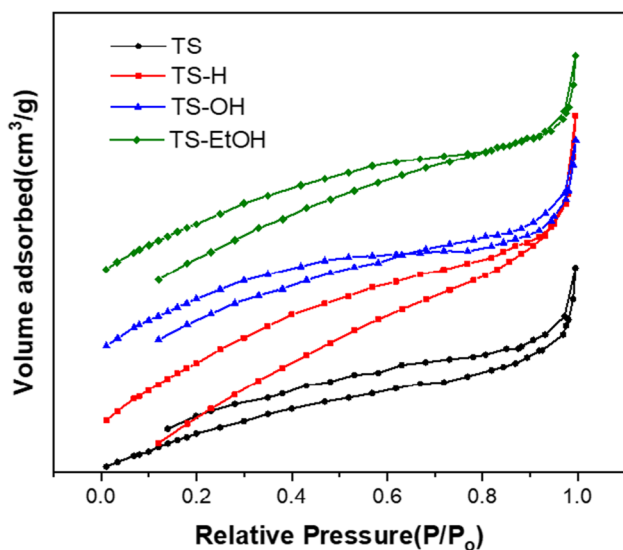
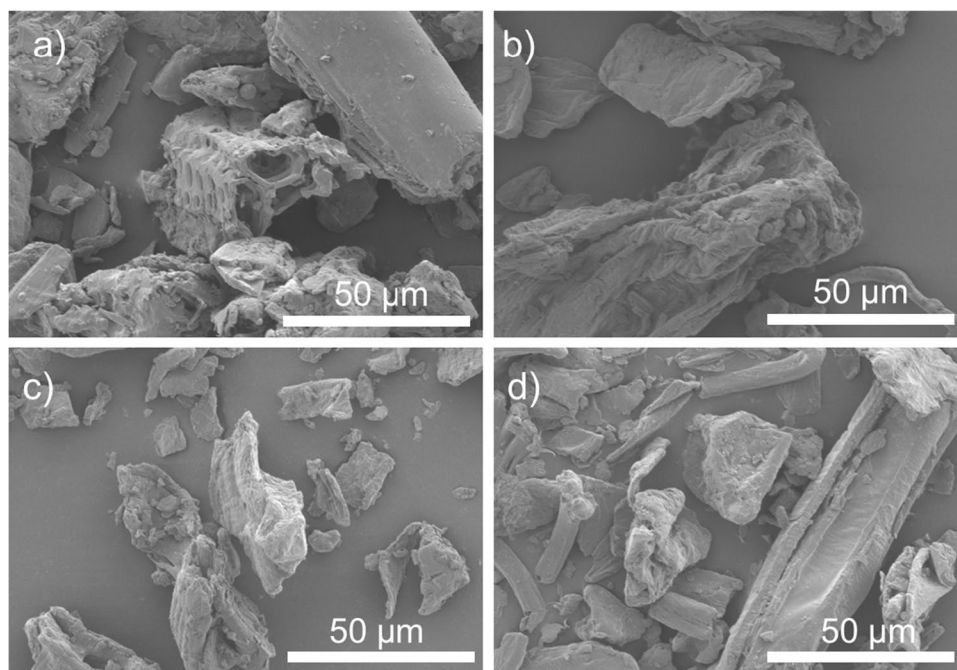


**Fig. 2** Adsorption and desorption isotherms in nitrogen gas for the raw and washed TS samples

structure was destroyed to some extent, which may be due to the swelling effect and removal of cross-linking components during the acid and alkaline washing treatments. The adsorption-desorption isotherms of the TS samples are shown in Fig. 2. Meanwhile, the pore structure characteristics results are presented in Table 4. It can be seen that solvents treatment increased the surface area and pore volume of the raw TS. This phenomenon may be caused by two reasons. The dissolution of soluble components in TS and disrupted

**Table 4** The surface area and pore size characterization of the TS samples

Sample	$S_{\text{BET}}(\text{m}^2/\text{g})$	$V_{\text{BJH}}(\text{cm}^3/\text{g})$
TS	2.89	0.0041
TS-H	4.75	0.0064
TS-OH	3.83	0.0049
TS-EtOH	3.70	0.0045

cellulose structure by acid or base reagent may contribute to the increase of surface area together.

To further understand the surface chemical variations in the TS after solvent pretreatment, FTIR analysis was investigated for the samples, and the result was shown in Fig. 3. The biomass TS was mainly composed of cellulose, hemicellulose, lignin, and a small amount of low boiling point non-polymeric components (such as pectin, protein, polyphenol) [30, 34, 35]. The absorption bands around  $3382\text{ cm}^{-1}$  and  $2928\text{ cm}^{-1}$  were ascribed to the stretching vibration of -OH and aliphatic C-H, respectively. The band at  $1617\text{ cm}^{-1}$  with a shoulder at  $1728\text{ cm}^{-1}$  was associated with the C=O stretching vibration in aliphatic ketone, amide, and carboxylic groups [36]. The bands at  $1424\text{ cm}^{-1}$  and  $1320\text{ cm}^{-1}$  could be attributed to C=C stretching of aromatic groups and breathing vibrations of syringyl units in lignocellulosic biomass, respectively. In addition, the wideband at approximately  $1056\text{ cm}^{-1}$  was ascribed to C-O-C stretching vibrations in cellulose and hemicellulose. These infrared peaks are the typical representative of biomass samples.

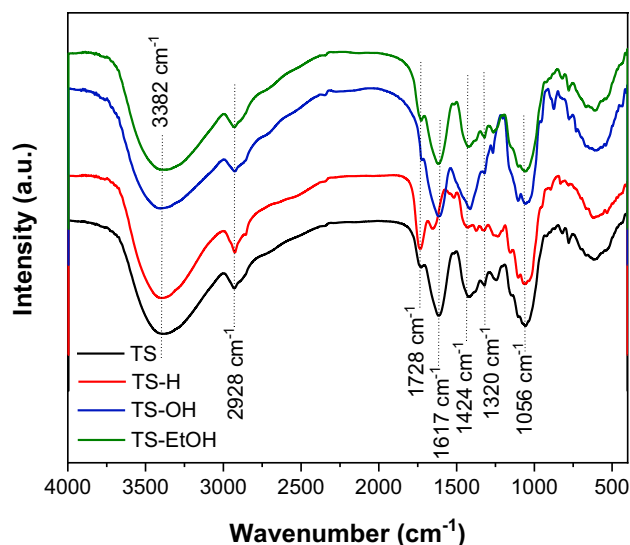


**Fig. 3** FTIR spectra of the raw and washed TS samples

By comparing the spectra of the four samples, it can be seen that the solvent pretreatment changed the organic functional groups on the surface of TS to some extent. A significant enhancement of the band intensity at  $1728\text{ cm}^{-1}$  accompanied by a weakened intensity at  $1617\text{ cm}^{-1}$  was observed after the acid washing. This phenomenon can be attributed to the fact that the highly polymerized lignin structure was partially disrupted and decomposed into species with aliphatic ketones, amides, and carboxylic groups. In addition, the intensity of the bands at  $1728\text{ cm}^{-1}$  and  $1320\text{ cm}^{-1}$  were found to considerably weaken after alkaline washing, which indicated that the lignin in the cross-linking structure can be damaged by hydroxide [37]. Alkaline washing also led to an increase in the intensity of the band at  $1056\text{ cm}^{-1}$ , implying that the exposure of the cellulose components increased by the removal of soluble substance during the alkaline washing pretreatment.

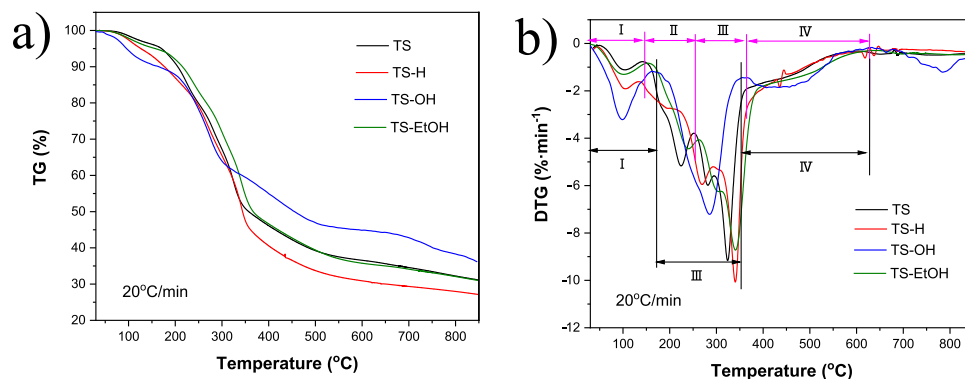
Moreover, the washing pretreatment with ethanol had little effect on the change of surface structure.

### 3.2 Pyrolysis characteristic analysis of the TS samples

The pyrolysis behaviors of the TS samples were analyzed through TG, and the profiles and corresponding DTG curves at the heating rate of  $20\text{ °C/min}$  are presented in Fig. 4. The pyrolysis of TS was a very complicated physical and chemical reaction process, which mainly related to the moisture dehydration, decomposition of tobacco non-polymeric constituents with the low boiling point, and decomposition of biopolymers such as hemicellulose, cellulose, and lignin [38]. It can be observed from the DTG curve of raw TS that the whole pyrolysis process consisted of four stages (I–IV) according to the temperature intervals. In stage I, the mass loss of 3.65% was caused by the evaporation of water. In stage II, the thermal decomposition of non-polymeric tobacco constituents such as sugar, pectin, and nicotine occurred between 147 and  $252\text{ °C}$ . In stage III, two peaks in the range of 252 and  $362\text{ °C}$  were clearly observed, which correspond to the decomposition of hemicellulose and cellulose respectively. In this stage, the mass loss rate increased greatly to compared with that of stage II. The stage IV was corresponded to the decomposition of lignin and carbonization process. In this stage, the mass loss rate was 12.77%, which indicated that lignin had high thermal stability due to its highly cross-linked structure. The mass loss higher than  $600\text{ °C}$  was ascribed to the decomposition of endogenous inorganic salts.

However, as for the solvent washed samples, it can be seen from the DTG curves that the pyrolysis process of TS-H and TS-OH were significantly different from that of raw TS. This may be caused by the changed physical structure and chemical composition of the TS after the corresponding pretreatments. As for TS-H sample, the DTG peak in stage II was almost disappeared, probably caused by the greatly removal of non-polymeric components such as pectin and

**Fig. 4** TG and DTG curves of the raw and washed TS samples



polyphenols during the acid washing process. As for the TS-OH sample, the stages II and III of raw TS combined into one decomposition stage in the temperature range of 163–343 °C under the heating rate of 20 °C/min, which may imply that significantly changed the lignocellulosic structure of biomass. Alcohol washing exhibited insignificant effect on the weight loss stage of pyrolysis of TS.

Furthermore, the TG-DTG curves of the raw and washed TS samples at different heating rates are shown in Fig. 5. And the temperature ranges and mass loss at different stages for various samples under different heating rates are summarized in Table 5. It can be seen that, with the heating rate increased, the temperature intervals of different stages shifted to higher temperatures due to the thermal hysteresis

**Fig. 5** TG and DTG curves of the raw and washed TS samples at different heating rates

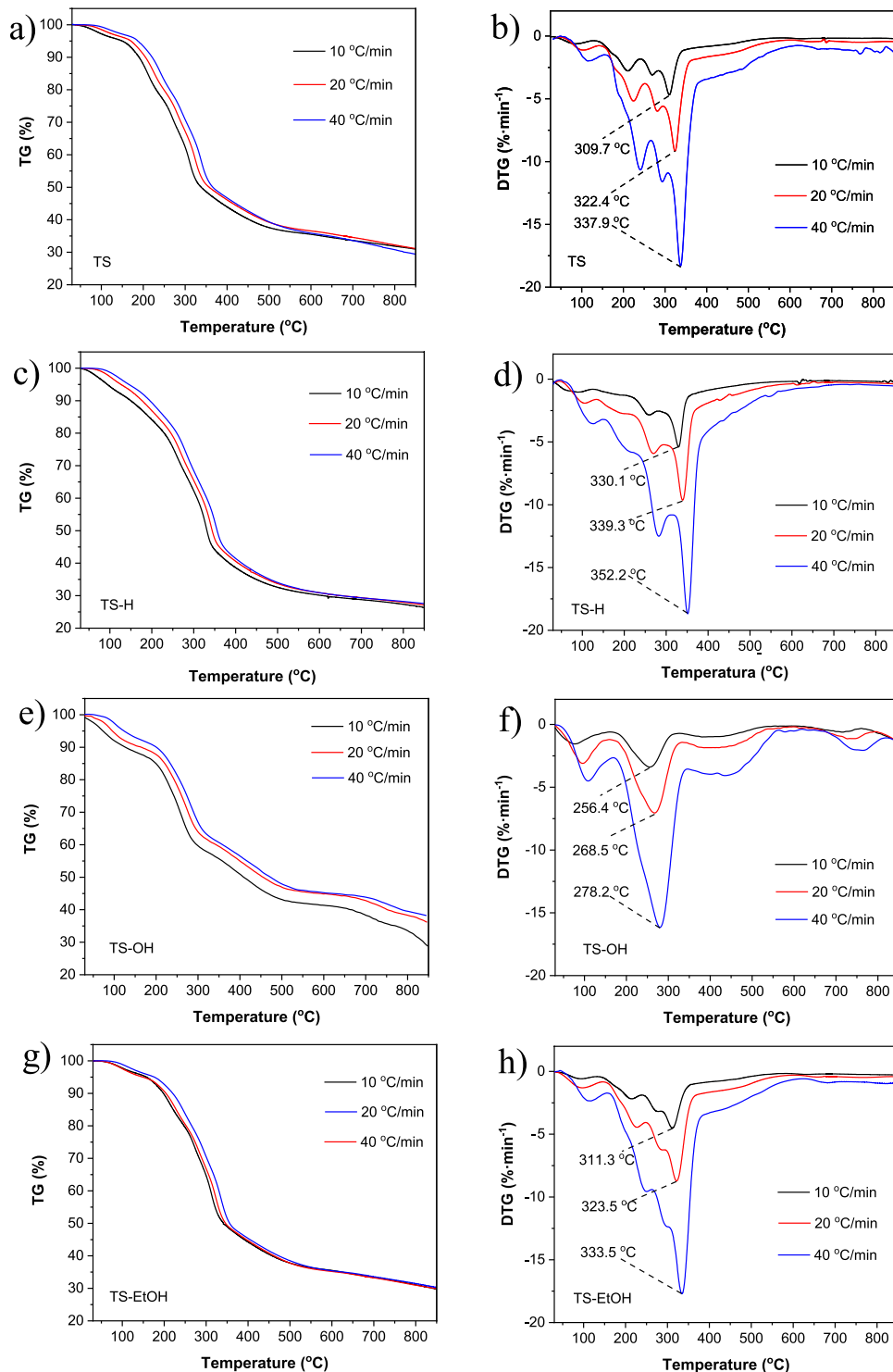


**Table 5** Temperature range and mass loss rate at different stages during the pyrolysis of the raw and washed TS samples

Sample	Heating rate (°C/min)	Stage I		Stage II		Stage III		Stage IV	
		Temperature	Mass loss	Temperature	Mass loss	Temperature	Mass loss	Temperature	Mass loss
		intervals (°C)	rate (%)	intervals (°C)	rate (%)	intervals (°C)	rate (%)	intervals(°C)	rate (%)
TS	10	40–135	4.22	135–246	18.52	246–340	27.44	340–560	13.65
	20	40–147	3.65	147–252	16.83	252–362	29.98	362–589	12.77
	40	40–160	3.27	160–267	17.51	267–381	30.80	381–620	12.93
TS-H	10	40–130	7.86	130–205	8.30	205–366	41.60	366–588	11.75
	20	40–135	5.66	135–216	9.59	216–377	41.77	377–600	12.05
	40	40–150	5.39	150–235	10.26	235–390	41.83	390–619	11.96
TS-OH	10	40–161	10.60	-	-	161–328	31.11	328–580	15.98
	20	40–163	9.54	-	-	163–343	30.23	343–588	15.00
	40	40–169	8.13	-	-	169–352	31.43	352–613	15.34
TS-EtOH	10	40–133	3.74	133–240	14.82	240–357	33.16	357–564	12.13
	20	40–147	4.90	147–248	14.25	248–366	33.18	366–587	12.28
	40	40–160	4.25	160–265	15.59	265–385	33.49	385–618	11.53

effect. In addition, the increased heating rate significantly increased the  $DTG_{max}$  in each stage for samples; this indicated that the rate of volatilization and pyrolysis of the samples increased along with the rate of heating. As for the percentage of mass loss at stage II and III, it can be seen that solvents pretreatment decreased the mass loss at stage II. This may be caused by the dissolution and extraction effect of soluble components during the washing process. At the same time, the mass loss at stage III increased to some extent due to the relative stability of cellulosic components. However, the TS-OH sample exhibited the minimum increase in the mass loss accompanied with a significantly decreased  $DTG_{max}$  at this stage, which may be related to the fact that cellulose pyrolysis is strongly dependent on the existence of sufficient inorganic species, which will typically reduce the reaction intensity [39]. Moreover, as for the stage IV, that

is the decomposition of lignin and carbonization stage, it can be seen that only the TS-OH sample exhibited an obvious difference in the weight loss process. The temperature interval of stage IV shifted to low temperature along with an increase of the weight loss, which may be related to the destructive effect on lignocellulosic structure during alkali washing process and the catalytic effect of residual sodium ion.

The pyrolysis characteristic parameters ( $T_i$ ,  $T_f$ ,  $T_m$ , and  $\eta$ ) of the raw and washed TS samples are summarized in Table 6. Acid and alkali pretreatments significantly increased the  $T_i$  of samples due to the removal of volatile components. The  $T_m$  at stage III for the TS-H sample increased 14.3–20.4 °C depending on the heating rate, while the  $T_m$  of TS-OH sample at this stage decreased significantly when compared with that of raw TS. In addition,

**Table 6** Pyrolysis characteristic parameters of TS samples

Sample	Heating rate (°C/min)	$T_i$ (°C)	$T_m$ (°C)		$T_f$ (°C)	CPI ( $10^{-4}\%/(\text{min}/^\circ\text{C}^2)$ )	Residues $\eta$ (%)
			Stage II	Stage III			
TS	10	161.4	208.9	309.7	348.3	0.81	30.99
	20	178.2	223.0	322.4	360.2	1.55	31.15
	40	190.7	240.3	337.9	376.0	2.97	29.38
TS-H	10	194.4	186.0	330.1	364.0	0.96	26.50
	20	195.6	190.3	339.3	375.3	1.65	27.13
	40	204.3	205.6	352.2	394.9	2.89	27.58
TS-OH	10	210.4	-	256.4	327.4	1.15	29.24
	20	199.4	-	268.5	335.4	1.93	36.30
	40	206.2	-	278.2	357.2	3.93	38.16
TS-EtOH	10	168.7	215.6	311.3	346.2	0.80	29.73
	20	178.4	226.0	323.5	356.5	1.51	29.93
	40	194.6	248.9	333.5	371.5	3.00	30.30



the  $T_f$  also exhibited the same trend with  $T_m$  for the TS-H and TS-OH samples. This phenomenon indicated a different effect of acid and alkali washing on the cellulosic structure and its pyrolysis process. It can be inferred that acid washing destroyed the structure of cellulose microfibrers in amorphous region, leading to an increased expose of fibers with high thermal stability in the crystalline region. In addition, the increased surface area and pore volume of TS-H may also contribute to this phenomenon due to the decreased heat transfer effect of TS-H. While the alkali washing may destroy the hydrogen bond network in the crystalline cellulose structure and promote the decomposition and dissolution of the cellulose structure, which can be reflected by the sharp decreased  $T_m$  at stage III, on the other hand, the alkali metal contents in the samples may also contribute to the above mentioned phenomenon through the catalysis effect [40, 41]. As for the TS-EtOH sample, there is a slight increase in the  $T_i$  and  $T_m$  of stage II, and the  $T_m$  of stage III was almost unchanged compared with that of raw TS, indicating a moderate effect of alcohol washing on the structure of TS.

Comprehensive pyrolysis index (CPI) was calculated in order to quantitatively compare the comprehensive pyrolysis characteristics. It can be seen that the CPI increased with the heating rate, indicating an enhanced pyrolysis property of TS under higher heating rate. In addition, the CPI of samples was significantly increased after the acid and alkali washing pretreatment, especially for the TS-OH sample, suggesting the positive effect of acid and alkali washing on the pyrolytic characteristic through the change of compositions and microstructure of biomass materials, while the CPI exhibited

a slight decrease as for the TS-EtOH samples. Moreover, the char residues rate ( $\eta$ ) during the pyrolysis process decreased after acid washing, while it increased after alkaline washing. This phenomenon may be related to changes of inorganic species in the biomass materials, which played an important role in the formation of char process [42].

### 3.3 FTIR analysis of pyrolytic gaseous products

The 3D FTIR spectrum of the released gas during pyrolysis process is shown in Fig. 6. On the whole, the appearance of absorbance peaks with time was consistent with the mass loss in the above DTG curves. The 3D spectra of the four samples demonstrated similar gaseous release behavior with some slight differences. In order to identify the components of the gaseous products, the 2D FTIR spectra at the peak temperature of the stage II and stage III are shown in Fig. 7. Based on the FTIR spectra, the result of component identification of the gaseous products is shown in Table 7. According to the FTIR spectra and previous reports [43], the volatile components can be divided into permanent gaseous components and organic components. In particular, the permanent gaseous components, such as  $H_2O$ ,  $CH_4$ ,  $CO_2$ , and  $CO$ , were readily identified by their characteristic bands. The release of organic components can also be identified between the wavenumber of  $1900\text{ cm}^{-1}$  and  $1000\text{ cm}^{-1}$ . The absorption band at  $1900\text{--}1650\text{ cm}^{-1}$  corresponds to the stretching vibrations of  $C=O$  which represents the formation of aldehydes, ketones, and acids [44], while it is difficult to identify each compound due to the complexity of components. The absorption band between  $1590$  and  $1450\text{ cm}^{-1}$  can be

**Fig. 6** 3D-FTIR images of pyrolysis of the raw and washed TS samples: **a** TS; **b** TS-H; **c** TS-OH; **d** TS-EtOH

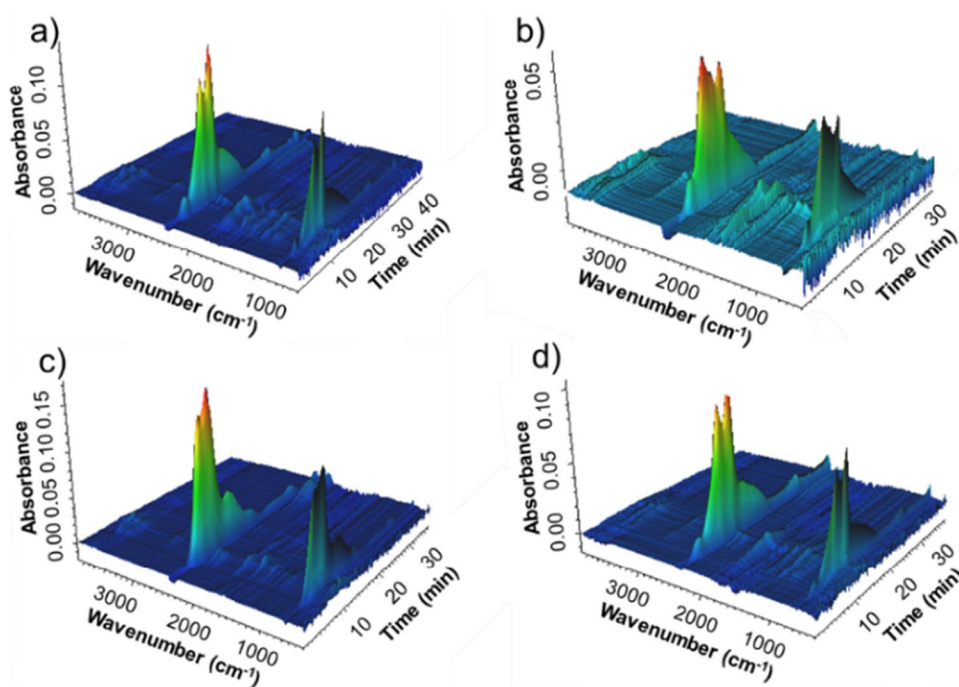


**Fig. 7** FTIR spectra of volatile products at peak temperature for the raw and washed TS samples

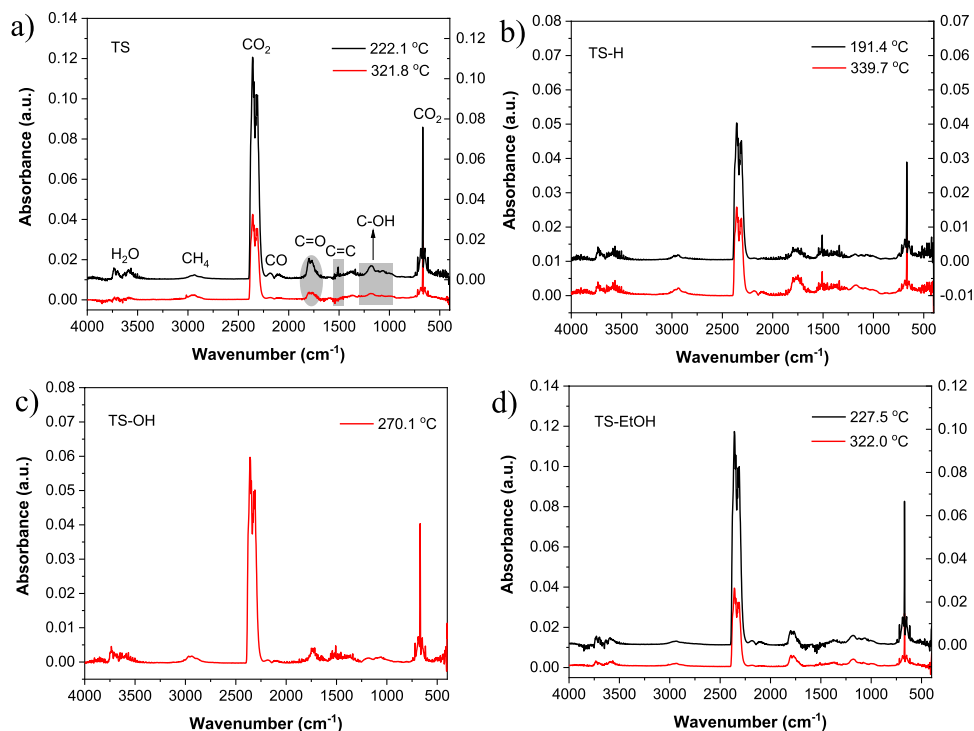


**Table 7** Gaseous products and functional groups during the pyrolysis of the raw and washed TS samples

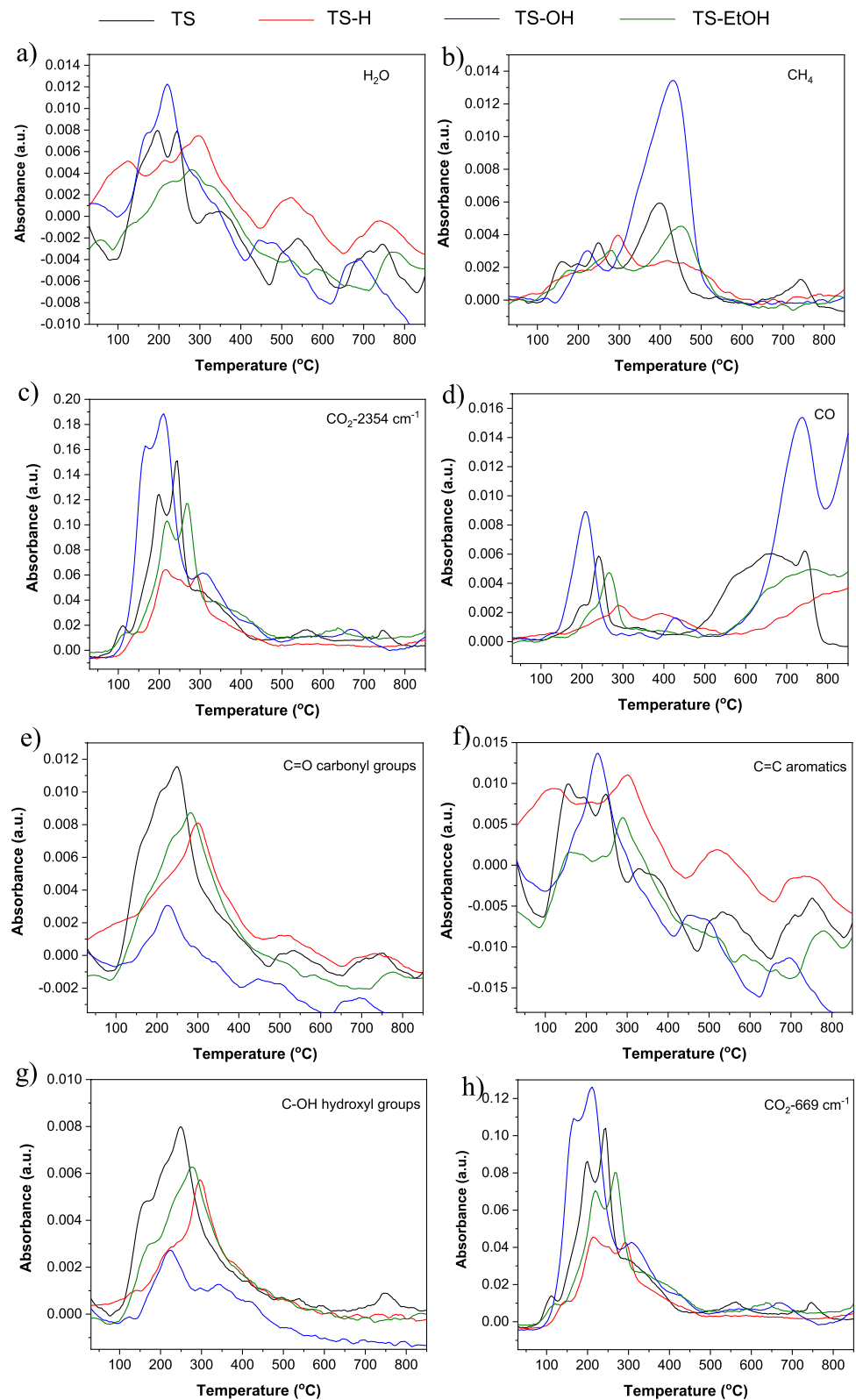
Compounds	Wavenumber (cm <sup>-1</sup> )	Functional groups	Vibrations
H <sub>2</sub> O	4000~3500	O-H	Stretching
CH <sub>4</sub>	3100~2700	C-H	Stretching
CO <sub>2</sub>	2400~2250/750~600	C=O	Stretching
CO	2250~2000	C-O	Stretching
Carbonyl groups	1900~1650	C=O	Stretching
Aromatics	1590~1450	C=C/benzene skeleton	Stretching
Hydroxyl groups	1280~970	C-OH	Stretching

assigned to the vibration of C=C stretching and benzene skeleton, which indicated the production of aromatics during pyrolysis process. The wavenumber between 1475 and 1000 cm<sup>-1</sup> is the fingerprint region, where the absorption band between 1280 and 970 cm<sup>-1</sup> can be attributed to the C-OH stretching vibration of alcohols and phenols. According to the widely used Lambert-Beer law, the absorbance at a specific wavenumber is linearly related to the concentration of formed gaseous products. It can be seen from Fig. 7 that the released CO<sub>2</sub> possessed the highest concentration for all the four samples during pyrolysis process.

Fig. 8 compares the evolution of gaseous products with increasing temperatures during the pyrolysis of the TS samples. As for the raw TS sample, it can be seen that the release of H<sub>2</sub>O varied with the temperature; the band below 200 °C was associated with the evaporation of water. The maximum release between 200 and 350 °C was mainly attributed to the cleavage of hydroxyl groups

in the lateral chains of the hemicellulose and cellulose [45]. Meanwhile, moisture was also produced during the pyrolysis of lignocellulosic components. CH<sub>4</sub> was formed by the cleavage of methoxy groups and methylene groups. This band showed a maximum release intensity between 400 and 500 °C, which was associated with the decomposition of lignin. The formation of CO<sub>2</sub> was attributed to the cracking of sugars, aldehydes, and acids in cellulose and hemicellulose at low temperatures, while the breaking of carboxyl and carbonyl groups in lignin at high temperatures also released small amounts of CO<sub>2</sub>. As can be seen from the Fig. 8c, the release of CO<sub>2</sub> mainly occurred in the low-temperature region below 400 °C. The released CO can be attributed to the cracking of ester bonds and carbonyl groups in sugars, and CO can also be generated by the reduction reaction of CO<sub>2</sub> with C at high temperatures [46]. A peak was observed between 200 and 300 °C which suggested that the formation of CO was related to

**Fig. 8** Evolution of different gaseous products with temperature during the pyrolysis of the raw and washed samples



the decomposition of hemicellulose, and the release of CO increased significantly above 600 °C. The release of CO was consistent with the study of Baker [47], which

suggested that the formation of carbon oxides occurred in two regions. The release curves for carbonyl and hydroxyl compounds were consistent in the maximum mass loss

**Table 8** Fitting results based on the Coats-Redfern model

Sample	Heating rate (°C/min)	Stage	Reaction model	Fitted equation	Coefficient $R^2$	Activation energy $E_a$ (kJ/mol)	Pre-exponential factor $A$ ( $\text{min}^{-1}$ )
TS	10	Stage II	F3/2	$y = 11827.31x + 12.3512$	0.9574	98.33	$2.73 \times 10^{10}$
	10	Stage III	F3/2	$y = 19066.9x + 20.74927$	0.9366	158.52	$1.96 \times 10^{14}$
	10	Stage IV	F3/2	$y = 10861.21x + 2.37511$	0.9241	90.30	$1.17 \times 10^6$
	20	Stage II	F3/2	$y = 12741.44x + 13.72441$	0.9554	105.93	$2.33 \times 10^{11}$
	20	Stage III	F3/2	$y = 17429.89x + 17.16158$	0.9488	144.91	$9.90 \times 10^{12}$
	20	Stage IV	F3/2	$y = 11353.5x + 2.41834$	0.9261	94.39	$2.55 \times 10^6$
	40	Stage II	F3/2	$y = 13133.41x + 13.6604$	0.9553	109.19	$4.50 \times 10^{11}$
	40	Stage III	F3/2	$y = 17658.12x + 16.71714$	0.9542	146.81	$1.29 \times 10^{13}$
	40	Stage IV	F3/2	$y = 6749.71x - 2.85435$	0.9264	93.55	$2.48 \times 10^6$
TS-H	10	Stage II	F3/2	$y = 12611.13x + 16.00349$	0.9212	104.85	$1.12 \times 10^{12}$
	10	Stage III	F3/2	$y = 10753.01x + 6.21139$	0.9347	89.40	$5.36 \times 10^7$
	10	Stage IV	F3/2	$y = 10689.94x + 1.58038$	0.9030	88.88	$5.24 \times 10^{11}$
	20	Stage II	F3/2	$y = 12231.53x + 14.57669$	0.9311	101.69	$5.24 \times 10^{11}$
	20	Stage III	F3/2	$y = 11067.84x + 6.40059$	0.9363	92.02	$1.33 \times 10^8$
	20	Stage IV	F3/2	$y = 11183.65x + 1.95528$	0.9131	92.98	$1.58 \times 10^6$
	40	Stage II	F3/2	$y = 12598.05x + 14.24477$	0.9386	104.74	$7.74 \times 10^{11}$
	40	Stage III	F3/2	$y = 12119.44x + 7.67519$	0.9368	100.76	$1.04 \times 10^9$
	40	Stage IV	F3/2	$y = 11193.06x + 1.63216$	0.9118	93.06	$2.29 \times 10^6$
TS-OH	10	Stage II	-	-	-	-	-
	10	Stage III	F3/2	$y = 10561.02x + 7.55511$	0.9813	87.80	$2.02 \times 10^8$
	10	Stage IV	F3/2	$y = 10929.03x + 2.44344$	0.9555	90.86	$1.26 \times 10^6$
	20	Stage II	-	-	-	-	-
	20	Stage III	F3/2	$y = 9854.55x + 5.81992$	0.9831	81.93	$6.64 \times 10^7$
	20	Stage IV	F3/2	$y = 11558.42x + 3.02967$	0.9534	96.10	$4.78 \times 10^6$
	40	Stage II	-	-	-	-	-
	40	Stage III	F3/2	$y = 9791.65x + 5.40653$	0.9796	81.41	$8.73 \times 10^7$
	40	Stage IV	F3/2	$y = 11130.64x + 2.08739$	0.9538	92.54	$3.59 \times 10^6$
TS-EtOH	10	Stage II	F3/2	$y = 11364.11x + 11.50925$	0.9522	94.48	$1.13 \times 10^{10}$
	10	Stage III	F3/2	$y = 16353.06x + 15.78571$	0.9536	135.96	$1.17 \times 10^{12}$
	10	Stage IV	F3/2	$y = 12026.54x + 3.67348$	0.9218	99.99	$4.74 \times 10^6$
	20	Stage II	F3/2	$y = 12612.2x + 13.49361$	0.9541	104.86	$1.83 \times 10^{11}$
	20	Stage III	F3/2	$y = 16451.55x + 15.52729$	0.9542	136.79	$1.82 \times 10^{12}$
	20	Stage IV	F3/2	$y = 11894.79x + 3.1178$	0.9281	98.89	$5.38 \times 10^6$
	40	Stage II	F3/2	$y = 12549.28x + 12.47816$	0.9502	104.33	$1.32 \times 10^{11}$
	40	Stage III	F3/2	$y = 17072.11x + 15.80365$	0.9608	141.94	$4.99 \times 10^{12}$
	40	Stage IV	F3/2	$y = 11732.05x + 2.36893$	0.9279	97.54	$5.01 \times 10^6$

range, indicating that the formation of aldehydes and ketones was accompanied by the formation of alcohols and phenols during pyrolysis process. In addition, aromatics were formed at temperatures between 200 and 350 °C, suggesting that the decomposition of hemicellulose and cellulose generated the aromatized structure.

Compared with raw TS, the release of  $\text{CH}_4$  increased significantly for TS-OH during the pyrolysis, which may indicate the destroyed structure of lignocellulose after the alkali washing pretreatment. The maximum release temperature of

$\text{CO}_2$  and CO shifted to lower temperatures and the amount of release increased significantly, which may be caused by the changed microstructure and catalytic effect of residual alkali metal during the pyrolysis process. The formation of aldehydes, ketones, acids, and phenols and alcohols were lower in the pretreated TS than those in the raw TS during pyrolysis process. A previous study found that the presence of K not only enhanced its catalytic effect on the ring-opening of cellulose to form carbonyl compounds such as aldehydes and ketones, but also increased the content of

phenolic products in the pyrolysis oils [48]. In addition, the aromatic compounds increased after acid and alkali pretreatment, which was attributed to the removal of sugars during acid and alkali washing, facilitating the aromatization and carbonization reaction.

### 3.4 Pyrolysis kinetic analysis

The Coats-Redfern method was used to describe the main thermal decomposition stage of the raw and washed TS samples, and the fitting results are listed in Table 8. Generally, 1.5-order reaction model (F1.5) had the highest correlation coefficients ( $R^2$ ) for the main decomposition stages of four samples at different heating rates. As for TS sample, the stage III exhibited the highest activation energy ( $E_a$ ) values (ranging from 144.91 to 158.52 kJ/mol) under different heating rates, which indicated that the decomposition of hemicellulose and cellulose with complex polymerization required higher temperature and higher energy. However, the  $E_a$  for the decomposition reactions in stage IV was the lowest. This phenomenon may be related to the developed pore structure that formed through the decomposition of cellulosic components in sample.

After the acid and alkaline washing pretreatment, the  $E_a$  values of stage III significantly decreased (especially for the TS-OH sample), which may be attributed to the broken structure of biomass. In addition, the more content of residual alkali metals in TS-OH sample may play a notable catalytic effect on the pyrolysis process, leading to a lowest  $E_a$  in stage III under any heating rates [49]. The  $E_a$  of the TS-EtOH in all stages were not quite different from those of TS, indicating that the alcohol washing had little effect on the structure of the biomass.

## 4 Conclusions

Among the three solvents, hydrochloric acid and sodium hydroxide exhibited notable effect on the composition and structure of TS, while ethanol had a weaker effect. Chemical composition analysis showed that the carbon content increased, while the hydrogen and oxygen content decreased after solvents pretreatment. The pretreated TS exhibited lower O/C, H/C, nitrogen, and sulfur, which was beneficial for the thermochemical utilization. SEM, BET, and FTIR analysis indicated that the acid and alkaline washing also changed the physical and surface chemical structure to some extent. Thermogravimetric analysis showed that solvents pretreatment increased the  $T_i$  of TS due to the removal of unstable volatile components. The  $T_m$  of cellulose decomposition process (stage III) increased, and the residual char decreased due to the destroyed structure of cellulosic structure and a reduction in catalytic reactions caused by inorganic species after acid

washing, while alkali washing significantly decreased the  $T_m$  at stage III due to the destroyed hydrogen bond network in the crystalline cellulose structure and the catalytic effect of residual alkali metal during the pretreatment process. The significantly increased CPI values of acid and alkali washed samples suggesting the positive effect of corresponding solvent pretreatment on the pyrolysis characteristics. The effect of solvents pretreatment on the change of structure and pyrolysis property was also reflected in the gaseous release behavior of CO<sub>2</sub>, CO, aldehydes, ketones, acids, phenols, and alcohols by TG-FTIR analysis. The pyrolysis kinetic behavior was studied through Coats-Redfern method. The raw and washed TS samples were controlled by F1.5 chemical reaction during pyrolysis process, and the acid and alkaline washing significantly decreased the  $E_a$  values of stage III (especially for the TS-OH sample), which may be attributed to the broken structure of biomass during the pretreatment process.

**Author contribution** All authors contributed to the study conception and design. The summary is as follows: Conceptualization: Miao Liang. Material preparation: Ming Han. Methodology: Xiao Li. Formal analysis and investigation: Qingqing Zhao, Wei Wang, Xuhe Wei. Writing—original draft preparation: Xiao Li, Qingqing Zhao. Writing—review and editing: Zhongya Guo, Miao Liang, Ke Zhang, Bin Li. Funding acquisition: Xiao Li, Ming Han. Supervision: Miao Liang, Zhongya Guo. All authors commented on previous versions of the manuscript. All authors read and approved the final manuscript.

**Funding** This work was supported by the the project (No. AW201922) from China Tobacco Henan Industrial Co., Ltd. and the Research Foundation (No. 2019ZCKJ304, 2014BSJJ067) of Zhengzhou University of Light Industry.

### Declarations

**Conflict of interest** The authors declare no competing interests.

## References

1. Wu W, Mei Y, Zhang L, Liu R, Cai J (2015) Kinetics and reaction chemistry of pyrolysis and combustion of tobacco waste. *Fuel* 156:71–80. <https://doi.org/10.1016/j.fuel.2015.04.016>
2. Gao W, Chen K, Xiang Z, Yang F, Zeng P, Li J, Yang R, Rao G, Tao H (2013) Kinetic study on pyrolysis of tobacco residues from the cigarette industry. *Ind Crop Prod* 44:152–157. <https://doi.org/10.1016/j.indcrop.2012.10.032>
3. Carlson TR, Cheng YT, Jae J, Huber GW (2011) Production of green aromatics and olefins by catalytic fast pyrolysis of wood sawdust. *Energy Environ Sci* 4(1):145–161. <https://doi.org/10.1039/c0ee00341g>
4. Zhang L, Liu R, Yin R, Mei Y (2013) Upgrading of bio-oil from biomass fast pyrolysis in China: a review. *Renew Sustain Energy Rev* 24:66–72. <https://doi.org/10.1016/j.rser.2013.03.027>
5. Carpenter D, Westover TL, Czernik S, Jablonski W (2014) Biomass feedstocks for renewable fuel production: a review of the impacts of feedstock and pretreatment on the yield and product



- distribution of fast pyrolysis bio-oils and vapors. *Green Chem* 16(2):384–406. <https://doi.org/10.1039/c3gc41631c>
6. Paulsen AD, Hough BR, Williams CL, Teixeira AR, Schwartz DT, Pfaendtner J, Dauenhauer PJ (2014) Fast pyrolysis of wood for biofuels: spatiotemporally resolved diffuse reflectance in situ spectroscopy of particles. *Chemosuschem* 7(3):765–776. <https://doi.org/10.1002/cssc.201301056>
  7. Talmadge MS, Baldwin RM, Biddy MJ, McCormick RL, Beckham GT, Ferguson GA, Czernik S, Magrini-Bair KA, Foust TD, Metelski PD et al (2014) A perspective on oxygenated species in the refinery integration of pyrolysis oil. *Green Chem* 16(2):407–453. <https://doi.org/10.1039/c3gc41951g>
  8. Abdullah H, Wu H (2009) Biochar as a fuel: 1. Properties and grindability of biochars produced from the pyrolysis of Mallee wood under slow-heating conditions. *Energy Fuel* 23(8):4174–4181. <https://doi.org/10.1021/ef900494t>
  9. Jung C, Park J, Lim KH, Park S, Heo J, Her N, Oh J, Yun S, Yoon Y (2013) Adsorption of selected endocrine disrupting compounds and pharmaceuticals on activated biochars. *J Hazard Mater* 263:702–710. <https://doi.org/10.1016/j.jhazmat.2013.10.033>
  10. Ahmad M, Rajapaksha AU, Lim JE, Zhang M, Bolan N, Mohan D, Vithanage M, Lee SS, Ok YS (2014) Biochar as a sorbent for contaminant management in soil and water: a review. *Chemosphere* 99:19–33. <https://doi.org/10.1016/j.chemosphere.2013.10.071>
  11. Manya JJ (2012) Pyrolysis for biochar purposes: a review to establish current knowledge gaps and research needs. *Environ Sci Technol* 46(15):7939–7954. <https://doi.org/10.1021/es301029g>
  12. Lehmann J (2007) A handful of carbon. *Nature* 447(7141):143–144. <https://doi.org/10.1038/447143a>
  13. Lin Y, Yan W, Sheng K (2016) Effect of pyrolysis conditions on the characteristics of biochar produced from a tobacco stem. *Waste Manag Res* 34(8):793–801. <https://doi.org/10.1177/0734242x16654977>
  14. Bushra B, Remya N (2020) Biochar from pyrolysis of rice husk biomass-characteristics, modification and environmental application. *Biomass Convers Biorefinery*: 1–12. <https://doi.org/10.1007/s13399-020-01092-3>
  15. Chen R, Zhang J, Lun L, Li Q, Zhang Y (2019) Comparative study on synergistic effects in co-pyrolysis of tobacco stalk with polymer wastes: thermal behavior, gas formation, and kinetics. *Bioresour Technol* 292:1–10. <https://doi.org/10.1016/j.biortech.2019.121970>
  16. Strezov V, Popovic E, Filkoski RV, Shah P, Evans T (2012) Assessment of the thermal processing behavior of tobacco waste. *Energy Fuel* 26(9):5930–5935. <https://doi.org/10.1021/ef3006004>
  17. Gomez-Siurana A, Marcilla BM, Berenguer D, Martinez-Castellanos I, Menargues S (2013) TGA/FTIR study of tobacco and glycerol-tobacco mixtures. *Thermochim Acta* 573:146–157. <https://doi.org/10.1016/j.tca.2013.09.007>
  18. Chen C, Luo Z, Yu C, Wang T, Zhang H (2017) Transformation behavior of potassium during pyrolysis of biomass. *RSC Adv* 7(50):31319–31326. <https://doi.org/10.1039/c7ra05162j>
  19. Taherzadeh MJ, Karimi K (2008) Pretreatment of lignocellulosic wastes to improve ethanol and biogas production: a review. *Int J Mol Sci* 9(9):1621–1651. <https://doi.org/10.3390/ijms9091621>
  20. Yao L, Yoo CG, Pu Y, Meng X, Muchero W, Tuskan GA, Tschaplinski TJ, Ragauskas AJ, Yang H (2019) Physicochemical changes of cellulose and their influences on *Populus trichocarpa* digestibility after different pretreatments. *BioResources* 14(4):9658–9676. <https://doi.org/10.15376/biores.14.4.9658-9676>
  21. Jiang L, Hu S, Xiang J, Su S, Sun L, Xu K, Yao Y (2012) Release characteristics of alkali and alkaline earth metallic species during biomass pyrolysis and steam gasification process. *Bioresour Technol* 116:278–284. <https://doi.org/10.1016/j.biortech.2012.03.051>
  22. Chen D, Cen K, Chen F, Ma Z, Zhou J, Li M (2020) Are the typical organic components in biomass pyrolyzed bio-oil available for leaching of alkali and alkaline earth metallic species (AAEMs) from biomass? *Fuel* 260:116347. <https://doi.org/10.1016/j.fuel.2019.116347>
  23. Cen K, Zhang J, Ma Z, Chen D, Zhou J, Ma H (2019) Investigation of the relevance between biomass pyrolysis polygeneration and washing pretreatment under different severities: water, dilute acid solution and aqueous phase bio-oil. *Bioresour Technol* 278:26–33. <https://doi.org/10.1016/j.biortech.2019.01.048>
  24. Chen Z, Leng E, Zhang Y, Zheng A, Peng Y, Gong X, Huang Y, Qiao Y (2018) Pyrolysis characteristics of tobacco stem after different solvent leaching treatments. *J Anal Appl Pyrolysis* 130:350–357. <https://doi.org/10.1016/j.jaap.2017.12.009>
  25. Sari NH, Wardana ING, Irawan YS, Siswanto E (2018) Characterization of the chemical, physical, and mechanical properties of NaOH-treated natural cellulosic fibers from corn husks. *J Nat Fibers* 15(4):545–558. <https://doi.org/10.1080/15440478.2017.1349707>
  26. Dalle D, Hansen B, Zattera AJ, Francisquetti EL, Catto AL, Borsoi C (2021) Kinetic evaluation of tobacco stalk waste exposed to alkaline surface treatment under different conditions. *Cellulose* 28(4):2053–2073. <https://doi.org/10.1007/s10570-020-03657-x>
  27. Cao Y, Zhou H, Fan J, Zhao H, Zhou T, Hack P, Chan C, Liou J, Pan W (2008) Mercury emissions during cofiring of sub-bituminous coal and biomass (chicken waste, wood, coffee residue, and tobacco stalk) in a laboratory-scale fluidized bed combustor. *Environ Sci Technol* 42(24):9378–9384. <https://doi.org/10.1021/es8016107>
  28. Fan Y, Li L, Tippayawong N, Xia S, Cao F, Yang X, Zhao Z, Li H (2019) Quantitative structure-reactivity relationships for pyrolysis and gasification of torrefied xylan. *Energy* 188:116119. <https://doi.org/10.1016/j.energy.2019.116119>
  29. White JE, Catallo WJ, Legendre BL (2011) Biomass pyrolysis kinetics: a comparative critical review with relevant agricultural residue case studies. *J Anal Appl Pyrolysis* 91(1):1–33. <https://doi.org/10.1016/j.jaap.2011.01.004>
  30. Cai J, Li B, Chen C, Wang J, Zhao M, Zhang K (2016) Hydrothermal carbonization of tobacco stalk for fuel application. *Bioresour Technol* 220:305–311. <https://doi.org/10.1016/j.biortech.2016.08.098>
  31. Liang M, Yang T, Zhang G, Zhang K, Wang L, Li R, He Y, Wang J, Zhang J (2021) Effects of hydrochloric acid washing on the structure and pyrolysis characteristics of tobacco stalk. *Biomass Convers Biorefinery* 1–14. <https://doi.org/10.1007/s13399-021-01616-5>
  32. Wang C, Li L, Chen R, Ma X, Lu M, Ma W, Peng H (2019) Thermal conversion of tobacco stem into gaseous products. *J Therm Anal Calorim* 137(3):811–823. <https://doi.org/10.1007/s10973-019-08010-4>
  33. Kuang M, Li Z (2014) Review of gas/particle flow, coal combustion, and NO<sub>x</sub> emission characteristics within down-fired boilers. *Energy* 69:144–178. <https://doi.org/10.1016/j.energy.2014.03.055>
  34. Reza MT, Yang X, Coronella CJ, Lin H, Hathwaik U, Shintani D, Neupane BP, Miller GC (2016) Hydrothermal carbonization (HTC) and pelletization of two arid land plants bagasse for energy densification. *ACS Sustain Chem Eng* 4(3):1106–1114. <https://doi.org/10.1021/acssuschemeng.5b01176>
  35. Abedi A, Cheng H, Dalai AK (2018) Effects of natural additives on the properties of sawdust fuel pellets. *Energy Fuel* 32(2):1863–1873. <https://doi.org/10.1021/acs.energyfuels.7b03663>
  36. Gao P, Zhou Y, Meng F, Zhang Y, Liu Z, Zhang W, Xue G (2016) Preparation and characterization of hydrochar from waste

- eucalyptus bark by hydrothermal carbonization. *Energy* 97:238–245. <https://doi.org/10.1016/j.energy.2015.12.123>
37. Oh GH, Yun CH, Park CR (2003) Role of KOH in the one-stage KOH activation of cellulosic biomass. *Carbon Lett* 4(4):180–184. <https://doi.org/10.1016/j.bmcl.2014.09.027>
38. Liang M, Zhang K, Lei P, Wang B, Shu C, Li B (2020) Fuel properties and combustion kinetics of hydrochar derived from co-hydrothermal carbonization of tobacco residues and graphene oxide. *Biomass Convers Biorefinery* 10(1):189–201. <https://doi.org/10.1007/s13399-019-00408-2>
39. Shimada N, Kawamoto H, Saka S (2008) Different action of alkali/alkaline earth metal chlorides on cellulose pyrolysis. *J Anal Appl Pyrolysis* 81(1):80–87. <https://doi.org/10.1016/j.jaap.2007.09.005>
40. Jiang L, Hu S, Sun L, Su S, Xu K, He L, Xiang J (2013) Influence of different demineralization treatments on physicochemical structure and thermal degradation of biomass. *Bioresour Technol* 146:254–260. <https://doi.org/10.1016/j.biortech.2013.07.063>
41. Le Brech Y, Ghislain T, Leclerc S, Bouroukba M, Delmotte L, Brosse N, Snape C, Chaimbault P, Dufour A (2016) Effect of potassium on the mechanisms of biomass pyrolysis studied using complementary analytical techniques. *Chemosuschem* 9(8):863–872. <https://doi.org/10.1002/cssc.201501560>
42. Nowakowski DJ, Jones JM, Brydson RMD, Ross AB (2007) Potassium catalysis in the pyrolysis behaviour of short rotation willow coppice. *Fuel* 86(15):2389–2402. <https://doi.org/10.1016/j.fuel.2007.01.026>
43. Ma Z, Chen D, Gu J, Bao B, Zhang Q (2015) Determination of pyrolysis characteristics and kinetics of palm kernel shell using TGA-FTIR and model-free integral methods. *Energy Convers Manag* 89:251–259. <https://doi.org/10.1016/j.enconman.2014.09.074>
44. Chen D, Cen K, Cao X, Chen F, Zhang J, Zhou J (2021) Insight into a new phenolic-leaching pretreatment on bamboo pyrolysis: release characteristics of pyrolytic volatiles, upgradation of three phase products, migration of elements, and energy yield. *Renew Sustain Energy Rev* 136:110444. <https://doi.org/10.1016/j.rser.2020.110444>
45. Zhou S, Xu YB, Wang CH, Tian ZF (2011) Pyrolysis behavior of pectin under the conditions that simulate cigarette smoking. *J Anal Appl Pyrolysis* 91(1):232–240. <https://doi.org/10.1016/j.jaap.2011.02.015>
46. Yuan T, Tahmasebi A, Yu J (2015) Comparative study on pyrolysis of lignocellulosic and algal biomass using a thermogravimetric and a fixed-bed reactor. *Bioresour Technol* 175:333–341. <https://doi.org/10.1016/j.biortech.2014.10.108>
47. Baker RR (1975) The formation of the oxides of carbon by the pyrolysis of tobacco. *Btrge Zur Tabakforschung* 8(1):16–27. <https://doi.org/10.2478/cttr-2013-0350>
48. Lu Q, Zhang Z, Yang X, Dong C, Zhu X (2013) Catalytic fast pyrolysis of biomass impregnated with  $K_3PO_4$  to produce phenolic compounds: analytical Py-GC/MS study. *J Anal Appl Pyrolysis* 104:139–145. <https://doi.org/10.1016/j.jaap.2013.08.011>
49. Pu G, Zhu W, Zhou H, Liu Y, Zhang Z (2015) Kinetics of co-gasification of low-quality lean coal and biomass. *BioResources* 10(2):2773–2782. <https://doi.org/10.15376/biores.10.2.2773-2782>

**Publisher's note** Springer Nature remains neutral with regard to jurisdictional claims in published maps and institutional affiliations.